Research in Astronomy and Astrophysics, 25:085002 (13pp), 2025 August
https://doi.org/10.1088/1674-4527/addded
CSTR: 32081.14.RAA.addded

Dynamic Evolution of the Eclipsing Overcontact Binary Star System BI CVn

İ. Bulut[1,2], M. Güneş[3,4], and Ç. Nehir[5]

[1] Department of Space Sciences and Technologies, Faculty of Sciences, Çanakkale Onsekiz Mart University, Terzioğlu Kampüsü, TR-17020, Çanakkale, Türkiye; ibulut@comu.edu.tr
[2] Astrophysics Research Centre and Observatory, Çanakkale Onsekiz Mart University, Terzioğlu Kampüsü, TR-17020, Çanakkale, Türkiye
[3] Space Science and Solar Energy Research and Application Center (UZAYMER), University of Çukurova, 01330, Adana, Türkiye; mumingunes@cu.edu.tr
[4] Adana Organised Industrial Zones Vocational School of Technical Science, University of Çukurova, 01410, Adana, Türkiye
[5] Türkiye National Observatory, TUG, Antalya, 07070, Türkiye
Received 2025 January 24; revised 2025 May 22; accepted 2025 May 23; published 2025 June 19

Abstract

We present a comprehensive analysis of BI CVn, an eclipsing overcontact binary system. New BVR photometric observations, combined with available spectroscopic data, were analyzed simultaneously using the Wilson–Devinney method to derive the orbital and physical parameters of the system. The resulting stellar parameters are $M_1 = 0.58 \pm 0.01 M_\odot$, $M_2 = 1.42 \pm 0.02 M_\odot$, $R_1 = 0.88 \pm 0.01 R_\odot$, $R_2 = 1.31 \pm 0.01 R_\odot$, with an orbital separation of $a = 2.80 \pm 0.01 R_\odot$. Based on all available CCD times of minimum light, including both ground-based and TESS observations, the $(O - C)$ diagram of BI CVn was analyzed. The orbital period exhibits a long-term decrease at a rate of $-2.3239\ (\pm 0.0001) \times 10^{-8}$ day yr^{-1}, likely due to mass transfer from the more massive to the less massive component. Superimposed on this trend is a cyclic variation with a period of 56.84 ± 0.08 yr, indicative of a light-travel time effect caused by a third body, whose estimated mass is $0.63 \pm 0.02 M_\odot$. Using these derived parameters, we modeled the binary's evolution through non-conservative processes with the Binary Star Evolution code. The evolutionary tracks of the components were examined in multiple parameter planes, leading to an estimated merger timescale of approximately 2.70 Gyr.

Key words: (stars:) binaries: eclipsing – stars: fundamental parameters – stars: individual BI CVn

1. Introduction

W UMa-type systems are eclipsing binary stars with orbital periods of less than a day which exhibit continuous variations in their light curves. These systems consist of two solar-type stars that are either nearly or fully in contact with one another. Both components have filled their own Roche lobes and are surrounded by a common convective envelope. Despite their advanced age, the components of W UMa-type systems exhibit rapid rotation. These systems may be progenitors of fast-rotating single stars known as blue stragglers, observed in star clusters (e.g., Samec et al. 2011). Due to the strong tidal interactions between the stars, their spins and orbits are synchronized. Additionally, they have the shortest orbital periods and lowest angular momentum of all main-sequence binary systems. It is predicted that these systems constantly lose angular momentum, causing their orbits to shrink and the stars to move closer together, ultimately leading to the merging of the two stars into a single entity (e.g., vant Veer 1979). The most significant observational evidence of this process is the discovery that Nova Sco, which erupted in 2008, resulted from the collision and merging of the binary components in V1309 Sco (Tylenda et al. 2011). Bulut & Aşkın (2022) found that 21% of W UMa systems brighter than $V = 10$ mag in the General Catalog of Variable Stars are triple systems. These are important systems for the study of the formation and evolution of multiple systems, as well as being unique astrophysics laboratories for the study of many physical phenomena such as orbital period change, gravitation, mass loss, mass transfer between components, orbital angular momentum evolution, etc.

BI Canum Venaticorum (BI CVn, NVS 6077 = BD +372356 = 2MASS J13031641+3637005 = GSC 2534−1628 = HIP 63701) was first identified as a variable star by Filatov (1960), who suggested that it may belong to the W UMa-type of eclipsing binary. The system has been studied by numerous authors (Zhukov 1982; Liu & Tan 1984, 1988; Demircan 1987; Maceroni & van't Veer 1996; Nelson et al. 2014) classified as a W-subtype W UMa binary and mass transfer was proposed as a reason for the increase in its orbital period. Maceroni & van't Veer (1996) later classified it as an A-subtype and determined its absolute parameters. Lu (1988) reported a mass ratio of 0.41 based on his spectroscopic observations. Finally, Nelson et al. (2014) performed the photometric and spectroscopic analysis of the system. These authors determined the photometric and absolute parameters by analyzing the light curves and radial velocity curves of BI CVn.

In this study, we present new CCD observations of BI CVn together with their photometric solutions. We also analyze the changes in the orbital period using all available eclipse times,

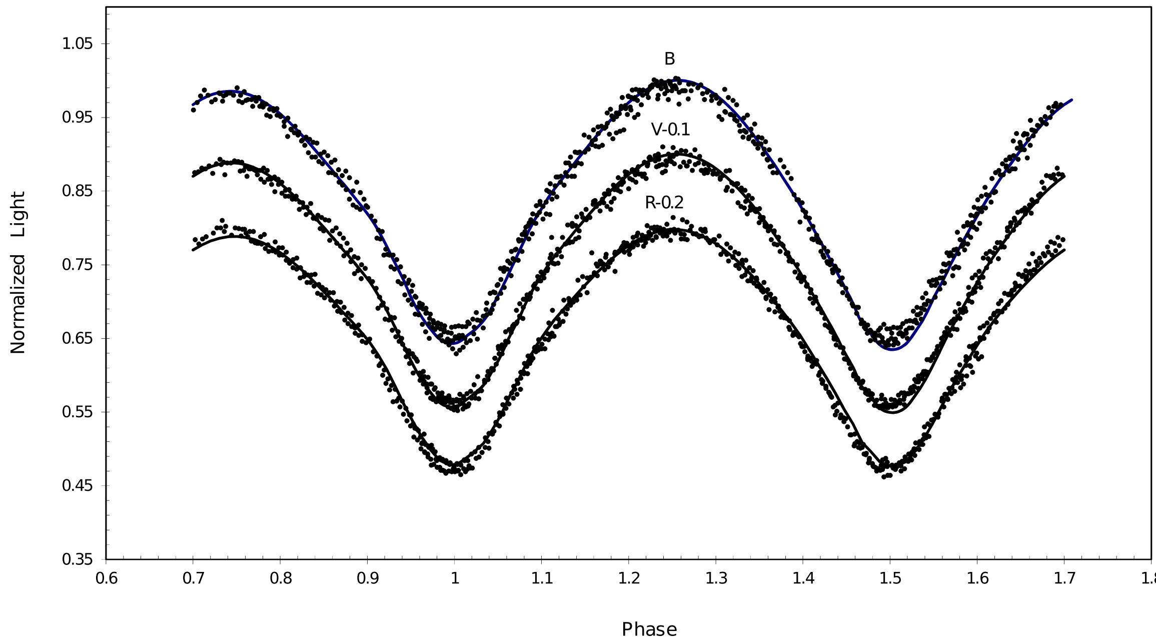

Figure 1. *B*, *V* and *R* observed (points) and theoretical (solid lines) light curves for BI CVn.

Table 1
Data for BI CVn and the Comparison and Check Stars

	System	R.A.	Decl.	*V* (mag)
V	BI CVn	$13^h03^m16\overset{s}{.}409$	$+36°37'00\overset{''}{.}645$	10.31
C1	GSC 2534 0151	$13^h03^m09\overset{s}{.}962$	$+36°35'19\overset{''}{.}12$	11.36
C2	GSC 2534 0434	$13^h01^m44\overset{s}{.}157$	$+36°34'57\overset{''}{.}79$	10.70

which show a combination of cyclical fluctuations and a continuously decreasing period. With the results found, we studied the dynamical evolution scenarios of the system and determined its initial orbital parameters.

2. CCD Photometric Observations

Photometric observations of BI CVn were conducted using an ALTAU47 CCD camera (E2V CCD47-10, Peltier cooling, 13 μm pixel size, 1024×1024 pixels) mounted on the 30 cm Schmidt–Cassegrain telescope (T30) at Çanakkale Onsekiz Mart University Ulupnar Observatory (COMUG). The observations were carried out over four nights-on 2015 April 12 and 28, and May 8 and 9. Johnson–Cousins *BVR* filters were used during the observations. Some catalog information for the eclipsing binary system (V), the comparison star (C1) and the check star (C2) from the SIMBAD database is presented in Table 1.

The observed CCD image reductions were made using the C-MUNIPACK software package (Motl 2007). The procedure for bias correction, flat-field correction, and aperture photometry was applied to all the CCD images.

From our new CCD observations with the *BVR* filters, a total of seven new times of light minima were determined, four of which were primary times of minima. The new times of minima and their uncertainties were calculated by the well-known method of Kwee & van Woerden (1956). For the times of minimum light obtained in *BVR* filters on the same observation night, average values were calculated. These minimum times were published by Bulut et al. (2017). *BVR* light curves of the system are displayed in Figure 1. The phases were calculated using the following linear light elements given by Nelson et al. (2014).

$$\mathrm{HJD(minI)} = 2456385.9752(3) + 0.3842100(1) x E. \quad (1)$$

3. Photometric Solutions

The light curves in the *BVR* bands, along with the radial velocity curves provided by Nelson et al. (2014) were analyzed together using The PHysics Of Eclipsing BinariEs (PHOEBE) code (version 0.31, Prša & Zwitter 2005), which is a computational implementation of the Wilson–Devinney (W–D) program (Wilson & Devinney 1971).

Nelson et al. (2014) collected spectroscopic data using the Cassegrain spectrograph attached on the 1.85 m Plaskett telescope at Dominion Astrophysical Observatory in Victoria, British Columbia, Canada. Their dataset includes a total of seven spectra of medium resolution.

The W–D program offers several modes to model different binary system configurations. In this study, Mode 3, representing an "over-contact binary not in thermal equilibrium," was chosen. The control parameter IPB was set to 1, which allows the

Table 2
Photometric Parameters of BI CVn

Description	Parameters	Value
The initial point of the ephemeris	T_0 (HJD)	2456385.9771 ± 0.0003
Orbital period	P (day)	0.384210
Semimajor axis	a ($R_\odot$)	2.80 ± 0.01
Center of mass velocity	V_γ (km s^{-1})	3.5 ± 0.1
Orbital inclination	i (deg)	70.08 ± 0.09
Temperature of primary comp.	M (K)	6125
Temperature of secondary comp.	T_2 (K)	6093 ± 100
Surface potential of components	$\Omega_1 = \Omega_2$	5.7538 ± 0.0054
Mass ratio	$q = M_2/M_1$	2.436 ± 0.003
The limb darkening of primary comp.	x_1	0.733
The limb darkening of secondary comp.	x_2	0.733
Bolometric albedo of components	$A_1 = A_2$	0.5
Gravity darkening of components	$g_1 = g_2$	0.32
The fractional luminosities of primary comp.	$L_1/(L_1 + L_2)$	0.330 ± 0.021(B)
		0.331 ± 0.022(V)
		0.320 ± 0.020(R)
The fractional luminosities of secondary comp.	$L_2/(L_1 + L_2)$	0.670(B)
		0.669(V)
		0.680(R)
The frac. radii of primary comp.	$r_{1,pole}$	0.2929 ± 0.0005
	$r_{1,side}$	0.3066 ± 0.0006
	$r_{1,back}$	0.3454 ± 0.0011
The frac. radii of secondary comp.	$r_{2,pole}$	0.4386 ± 0.0004
	$r_{2,side}$	0.4698 ± 0.0005
	$r_{2,back}$	0.4999 ± 0.0007
Fill-out factor	f (%)	17.1
	Spot Parameters	
Spot co-latitude	θ (rad)	1.256
Spot longitude	ϕ (rad)	0.6039
Spot radius	r (rad)	0.4791
Spot Temp. factor	$T_f = T_d/T_s$	0.965

decoupling of the secondary star's luminosity (L_2) and temperature (T_2), enabling independent adjustments of the luminosities of both stars (L_1 and L_2).

Several parameters were fixed during the analysis based on the system's known properties. The temperature of the primary star (T_1) was set to 6125 K, as determined by Nelson et al. (2014). The bolometric gravity-darkening coefficients ($g_1 = g_2$) and bolometric albedos ($A_1 = A_2$) were fixed at their theoretical values of 0.32 and 0.50, respectively, consistent with convective atmospheres (Lucy 1968). The monochromatic limb-darkening coefficients ($x_{1,2}$) were automatically interpolated by the PHOEBE code based on the tables provided by van Hamme (1993). A circular orbit was assumed, with the orbital eccentricity (e) set to 0 and the longitude of periastron (ω) fixed at 90°. Third light (l_3) was excluded from the analysis by setting it to 0. There is a clear asymmetry between the maxima of the light curve of BI CVn, suggesting the presence of the O'Connell effect (O'Connell 1951). To account for this effect, a cold spot on the secondary star was defined in the light curve solution.

Adjustable parameters included the reference epoch (T_0), orbital period (P), semimajor axis (a), systemic radial velocity (V_γ), orbital inclination (i), surface temperature of the secondary star (T_2), the dimensionless surface equipotential (Ω_1 and Ω_2), the mass ratio ($q = M_2/M_1$), and monochromatic luminosity of the primary star (L_1). The W–D program iteratively adjusted these parameters until the corrections for each free parameter fell below their respective standard deviations. The optimal parameters derived from the analysis are listed in Table 2. Figure 1 compares the observed light curves in *BVR* bands with the theoretical models, while Figure 2 displays the modeled radial velocity curves. The geometric configuration at phase 0.24 is displayed in Figure 3.

Nelson et al. (2014) performed light curve analysis for three sets of light curve data taken by different observers at different observatories. The light curve analysis results given in Table 2 are in reasonable agreement with the results of Nelson et al. (2014).

4. Changes in the Orbital Period

The investigation of orbital period variations plays a vital role in understanding the dynamical evolution of binary star systems, the existence of additional bodies, and the mass exchange between stellar components. Accordingly, studies on orbital period changes are of considerable significance in binary system research. The first detailed analysis of the orbital period variation of BI CVn was conducted by Qian et al. (2008) who reported a secular decrease in the orbital period at a rate of $dP/dt = -1.51(\pm 0.12) \times 10^{-7}$ day yr^{-1}. Furthermore, they identified a periodic oscillation with an amplitude of 0.151 days and a period of approximately 27.0 yr. This cyclic modulation was interpreted as the result of the light-travel time effect (LITE) due to a gravitationally bound third body. The minimum mass of this third component was estimated to be $0.58 M_\odot$.

In the present study, we constructed an updated $(O - C)$ diagram for BI CVn by compiling all available times of minimum light from the literature. During our photometric observations, we recorded seven eclipses, including four primary eclipses. Additionally, 491 minima times were obtained from TESS data. New minimum times and their

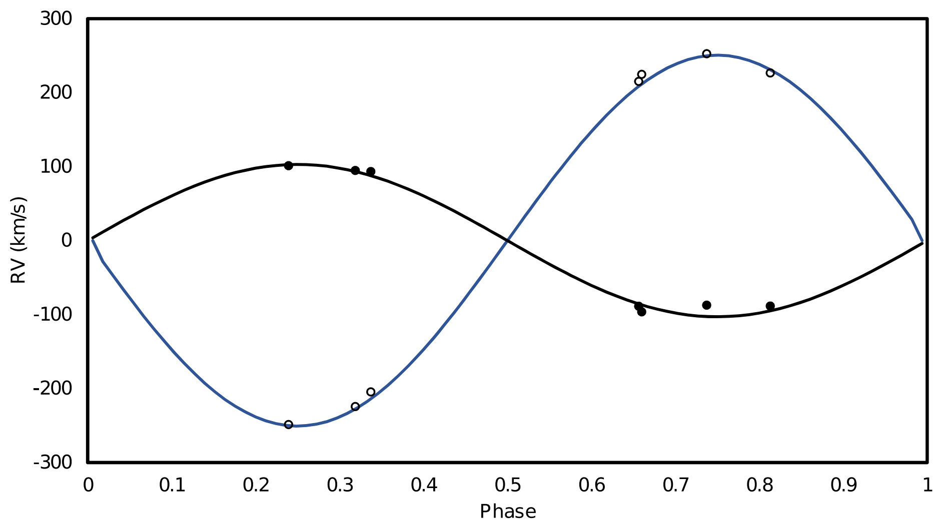

Figure 2. The fitted radial velocity curves (solid lines) for BI CVn are shown together with the observed data; filled circles symbolize the primary component and open circles symbolize the secondary component.

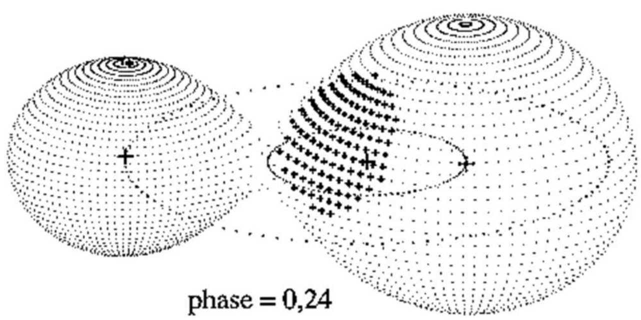

Figure 3. Roche lobes of BI CVn.

associated errors were calculated using the technique described by Kwee & van Woerden (1956). The TESS-based minimum times are listed in Table 3, while the others are presented in Table 4. Since TESS observation times are provided in Barycentric Julian Date (BJD), other observed minima were converted from Heliocentric Julian Date (HJD) to BJD using an online conversion tool (https://astroutils.astronomy.osu.edu/time/). As a result, a total of 719 minimum times were collected. The $(O-C)$ values were calculated using the linear ephemeris given in Equation (1). The resulting $(O-C)$ diagram, displayed in the upper panel of Figure 4, reveals cyclical variations superimposed on a parabolic trend, exhibiting a long-term orbital period decrease.

The $(O-C)$ analysis was conducted using the computer program developed by Zasche et al. (2009). A total of 707 observed minima times were included in the analysis, with observational weights assigned based on the observation method: visual data were weighted as 1, photographic data were weighted as 5, while photometric and CCD data were weighted as 10.

The parabolic variation observed in the $(O-C)$ diagram is typically attributed to mass transfer between the stellar components or mass loss from the binary system. This variation can be modeled using the following ephemeris

$$\mathrm{BJD(minI)} = 2456385.9929(18) + 0.38420923(12) \times E - 0.1217(1) \times 10^{-10} \times E^2 + \Delta t, \quad (2)$$

where the quadratic term indicates a steady decrease in the orbital period. The derived rate of period change is $dP/dt = 2Q/P = -2.3239\ (\pm 0.0001) \times 10^{-8}$ day yr^{-1}, consistent with ongoing mass transfer from the more massive to the less massive component.

Residuals from the parabolic fit reveal additional cyclic variations in the $(O-C)$ data. Such periodic modulations are generally attributed to one of two mechanisms: (1) magnetic activity cycles in one or both stars, or (2) LITE induced by an unseen tertiary component gravitationally bound to the system.

The periodic component of the $(O-C)$ diagram was modeled using the classical LITE formulation proposed by Irwin (1959)

$$\Delta t = \frac{a_{12} \sin i_3}{c} \times \left\{ \frac{1 - e_3^2}{1 + e_3 \cos \upsilon} \right\} \sin(\upsilon + \omega_3) + e_3 \cos \omega_3, \quad (3)$$

where a_{12} is the semimajor axis of the eclipsing binary's orbit around the center of mass of the triple system, i_3 is the inclination, e_3 the eccentricity, υ the true anomaly, and ω_3 the longitude of periastron. The parameters derived from the combined parabolic and LITE fit are presented in Table 5. The top panel of Figure 4 illustrates the best-fitting model superimposed on the $(O-C)$ data, while the residuals are shown in the bottom panel.

Table 3
Extracted Minima Times for BI CVn from TESS Database

Min+2400000 (BJD)	Error	Type	Min+2400000 (BJD)	Error	Type	Min+2400000 (BJD)	Error	Type
58899.48878	0.00009	p	58911.01406	0.00006	p	58923.69315	0.00004	p
58899.67966	0.00006	s	58911.20719	0.00008	s	58923.88569	0.00003	s
58899.87297	0.00007	p	58911.39820	0.00007	p	58924.07738	0.00004	p
58900.06392	0.00005	s	58911.59144	0.00008	s	58924.26988	0.00003	s
58900.25708	0.00005	p	58911.78242	0.00007	p	58924.46159	0.00004	p
58900.44813	0.00004	s	58911.97566	0.00008	s	58924.65411	0.00003	p
58900.64119	0.00004	p	58912.16663	0.00007	p	58924.84581	0.00004	s
58900.83234	0.00004	s	58912.35986	0.00008	s	58925.03836	0.00004	s
58901.02537	0.00004	p	58913.70388	0.00004	p	58925.23000	0.00004	p
58901.21660	0.00003	s	58913.89641	0.00009	s	58925.42254	0.00004	s
58901.40956	0.00003	p	58914.08809	0.00003	p	58925.61418	0.00004	p
58901.60086	0.00003	s	58914.28053	0.00006	s	58925.80670	0.00003	s
58901.79369	0.00003	p	58914.47233	0.00007	p	58925.99841	0.00004	p
58901.98514	0.00003	s	58914.66452	0.00004	s	58926.19088	0.00003	s
58902.17782	0.00002	p	58914.85641	0.00003	p	58926.38259	0.00004	p
58902.36943	0.00002	s	58915.04863	0.00003	s	58928.30365	0.00006	p
58902.56201	0.00002	p	58915.24061	0.00003	p	58928.49597	0.00004	s
58902.75367	0.00002	s	58915.43285	0.00004	s	58928.68789	0.00006	p
58902.94620	0.00002	p	58915.62479	0.00004	p	58928.88013	0.00004	s
58903.13789	0.00002	s	58915.81705	0.00003	s	58929.07197	0.00005	p
58903.33042	0.00002	p	58916.00896	0.00004	p	58929.26435	0.00003	s
58903.52212	0.00002	s	58916.20120	0.00003	s	58929.45626	0.00004	p
58903.71464	0.00002	p	58916.39322	0.00003	p	58929.64855	0.00003	s
58903.90634	0.00002	s	58916.58540	0.00002	s	58929.84045	0.00004	p
58904.09889	0.00002	p	58916.77745	0.00003	p	58930.03278	0.00003	s
58904.29055	0.00002	s	58916.96961	0.00002	s	58930.22466	0.00004	p
58904.48306	0.00002	p	58917.16162	0.00003	p	58930.41707	0.00004	s
58904.67474	0.00002	s	58917.35386	0.00003	s	58930.60888	0.00004	p
58904.86721	0.00002	p	58917.54579	0.00003	p	58930.80129	0.00003	s
58905.05895	0.00002	s	58917.73809	0.00003	s	58930.99309	0.00004	p
58905.25130	0.00002	p	58917.92999	0.00003	p	58931.18552	0.00003	s
58905.44317	0.00002	s	58918.12226	0.00003	s	58931.37728	0.00004	p
58905.63537	0.00002	p	58918.31420	0.00004	p	58931.56979	0.00004	s
58905.82745	0.00003	s	58918.50649	0.00003	s	58931.76143	0.00005	p
58906.01947	0.00004	p	58918.69837	0.00004	p	58931.95412	0.00004	s
58906.21171	0.00003	s	58918.89071	0.00003	s	58932.14566	0.00005	p
58906.40357	0.00004	p	58919.08253	0.00004	p	58932.33839	0.00004	s
58906.59597	0.00004	s	58919.27493	0.00003	s	58932.52995	0.00004	p
58906.78771	0.00004	p	58919.46680	0.00004	p	58932.72261	0.00004	s
58906.98021	0.00004	s	58919.65915	0.00003	s	58932.91415	0.00005	p
58907.17194	0.00004	p	58919.85107	0.00003	p	58933.10683	0.00004	s
58907.36442	0.00004	s	58920.04332	0.00002	s	58933.29839	0.00005	p
58907.55615	0.00004	p	58920.23530	0.00003	p	58933.49105	0.00004	s
58907.74868	0.00004	s	58920.42749	0.00002	s	58933.68266	0.00004	p
58907.94029	0.00005	p	58920.61952	0.00003	p	58933.87533	0.00005	s
58908.13293	0.00005	s	58920.81172	0.00002	s	58934.06694	0.00004	p
58908.32451	0.00005	p	58921.00368	0.00003	p	58934.25960	0.00005	s
58908.51720	0.00006	s	58921.19597	0.00002	s	58934.45111	0.00005	p
58908.70883	0.00005	p	58921.38786	0.00003	p	58934.64387	0.00006	s
58908.90148	0.00005	s	58921.58025	0.00002	s	58934.83528	0.00005	p
58909.09310	0.00005	p	58921.77210	0.00003	p	58935.02802	0.00006	s
58909.28575	0.00005	s	58921.96450	0.00003	s	58935.21955	0.00005	p
58909.47733	0.00005	p	58922.15630	0.00003	p	58935.41221	0.00005	s
58909.67002	0.00005	s	58922.34874	0.00003	s	58935.60378	0.00004	p
58909.86157	0.00005	p	58922.54051	0.00004	p	58935.79635	0.00006	s
58910.05427	0.00005	s	58922.73296	0.00003	s	58935.98799	0.00005	p
58910.24578	0.00004	p	58922.92472	0.00004	p	58936.18036	0.00004	s

Table 3
(Continued)

Min+2400000 (BJD)	Error	Type	Min+2400000 (BJD)	Error	Type	Min+2400000 (BJD)	Error	Type
58910.43854	0.00006	s	58923.11721	0.00003	s	58936.37216	0.00004	p
58910.62996	0.00005	p	58923.30892	0.00004	p	58936.56465	0.00003	s
58910.82282	0.00007	s	58923.50147	0.00003	s	58936.75635	0.00003	p
58936.94887	0.00003	s	58949.43473	0.00010	p	59644.85658	0.00008	p
58937.14052	0.00004	p	58949.62814	0.00008	s	59645.05002	0.00007	s
58937.33306	0.00003	s	58949.81900	0.00010	p	59645.24078	0.00008	p
58937.52468	0.00005	p	58950.01232	0.00008	s	59645.43422	0.00007	s
58937.71721	0.00003	s	58950.20331	0.00008	p	59645.62502	0.00008	p
58937.90889	0.00004	p	58950.39647	0.00007	s	59645.81843	0.00007	s
58938.10138	0.00004	s	58950.58755	0.00007	p	59646.00930	0.00007	p
58938.29303	0.00005	p	58950.78063	0.00006	s	59646.20266	0.00007	s
58938.48558	0.00004	s	58950.97183	0.00006	p	59646.39352	0.00007	p
58938.67717	0.00005	p	58951.16481	0.00005	s	59646.58686	0.00006	s
58938.86980	0.00004	s	58951.35615	0.00006	p	59646.77775	0.00007	p
58939.06129	0.00006	p	58951.54898	0.00004	s	59646.97103	0.00006	s
58939.25405	0.00005	s	58951.74043	0.00005	p	59647.16199	0.00006	p
58939.44537	0.00007	p	58951.93317	0.00004	s	59647.35523	0.00006	s
58939.63832	0.00006	s	58952.12473	0.00004	p	59647.54622	0.00006	p
58939.82949	0.00007	p	58952.31736	0.00004	s	59647.73944	0.00006	s
58940.02255	0.00006	s	58952.50902	0.00004	p	59647.93050	0.00005	p
58940.21368	0.00008	p	58952.70157	0.00004	s	59648.12361	0.00006	s
58940.40673	0.00006	s	58952.89329	0.00004	p	59648.31475	0.00005	p
58940.59791	0.00009	p	58953.08578	0.00003	s	59648.50777	0.00005	s
58940.79094	0.00006	s	58953.27756	0.00003	p	59648.69896	0.00005	p
58941.94365	0.00010	s	58953.46995	0.00003	s	59648.89198	0.00005	s
58942.13480	0.00012	p	58953.66181	0.00003	p	59649.08317	0.00005	p
58942.32790	0.00007	s	58953.85413	0.00003	s	59649.27621	0.00005	s
58942.51900	0.00009	p	58954.04606	0.00003	p	59649.46739	0.00005	p
58942.71209	0.00007	s	58954.23832	0.00003	s	59649.66045	0.00006	s
58942.90329	0.00008	p	58954.43030	0.00002	p	59649.85160	0.00005	p
58943.09636	0.00007	s	58954.62245	0.00002	s	59650.04465	0.00005	s
58943.28725	0.00011	p	58954.81450	0.00002	p	59650.23584	0.00006	p
58943.48063	0.00008	s	59637.55697	0.00008	p	59650.42884	0.00005	s
58943.67154	0.00010	p	59637.74961	0.00007	s	59651.58164	0.00008	s
58943.86484	0.00008	s	59639.28689	0.00009	s	59651.77273	0.00008	p
58944.05576	0.00010	p	59639.47783	0.00011	p	59651.96584	0.00007	s
58944.24908	0.00008	s	59639.67107	0.00008	s	59653.69414	0.00004	p
58944.43998	0.00009	p	59639.86203	0.00008	p	59653.88659	0.00007	s
58944.63329	0.00007	s	59640.05528	0.00008	s	59654.07855	0.00005	p
58944.82418	0.00009	p	59640.24621	0.00008	p	59654.27085	0.00005	s
58945.01749	0.00008	s	59640.43950	0.00008	s	59654.46278	0.00005	p
58945.20835	0.00009	p	59640.63039	0.00008	p	59654.65518	0.00007	s
58945.40172	0.00007	s	59640.82372	0.00007	s	59654.84711	0.00008	p
58945.59257	0.00009	p	59641.01459	0.00008	p	59655.03937	0.00005	s
58945.78590	0.00008	s	59641.20793	0.00008	s	59655.23146	0.00007	p
58945.97677	0.00009	p	59641.39878	0.00009	p	59655.42353	0.00005	s
58946.17006	0.00008	s	59641.59214	0.00007	s	59655.61530	0.00003	p
58946.36095	0.00009	p	59641.78295	0.00009	p	59655.80770	0.00004	s
58946.55429	0.00008	s	59641.97635	0.00008	s	59655.99940	0.00003	p
58946.74514	0.00010	p	59642.16714	0.00008	p	59656.19186	0.00004	s
58946.93851	0.00009	s	59642.36055	0.00007	s	59656.38371	0.00003	p
58947.12931	0.00010	p	59642.55136	0.00008	p	59656.57604	0.00003	s
58947.32273	0.00009	s	59642.74470	0.00007	s	59656.76797	0.00003	p
58947.51352	0.00010	p	59642.93556	0.00008	p	59656.96023	0.00003	s
58947.70698	0.00008	s	59643.12894	0.00006	s	59657.15223	0.00002	p
58947.89777	0.00010	p	59643.31977	0.00007	p	59657.34443	0.00002	s
58948.09118	0.00008	s	59643.51312	0.00006	s	59657.53645	0.00002	p

Table 3
(Continued)

Min+2400000 (BJD)	Error	Type	Min+2400000 (BJD)	Error	Type	Min+2400000 (BJD)	Error	Type
58948.28200	0.00010	p	59643.70400	0.00007	p	59657.72864	0.00003	s
58948.47542	0.00009	s	59643.89726	0.00006	s	59657.92063	0.00002	p
58948.66628	0.00010	p	59644.08817	0.00007	p	59658.11288	0.00003	s
58948.85968	0.00009	s	59644.28148	0.00006	s	59658.30481	0.00002	p
58949.05054	0.00009	p	59644.47236	0.00008	p	59658.49714	0.00003	s
58949.24395	0.00008	s	59644.66575	0.00007	s	59658.68901	0.00002	p
59658.88136	0.00003	s	60370.63174	0.00004	p	60383.11844	0.00003	s
59659.07328	0.00002	p	60374.47418	0.00004	p	60383.31128	0.00004	p
59659.26551	0.00002	s	60374.66575	0.00005	s	60383.50259	0.00003	s
59659.45753	0.00002	p	60374.85841	0.00003	p	60383.69550	0.00004	p
59659.64972	0.00002	s	60375.04992	0.00004	s	60383.88675	0.00004	s
59659.84176	0.00002	p	60375.24266	0.00004	p	60384.07972	0.00004	p
59660.03400	0.00002	s	60375.43411	0.00004	s	60384.27093	0.00004	s
59660.22599	0.00002	p	60375.62689	0.00003	p	60384.46394	0.00004	p
59660.41818	0.00002	s	60375.81833	0.00004	s	60384.65511	0.00004	s
59660.61024	0.00002	p	60376.01113	0.00004	p	60384.84818	0.00005	p
59660.80237	0.00002	s	60376.20257	0.00004	s	60385.03934	0.00006	s
59660.99449	0.00002	p	60376.39535	0.00004	p	60388.69012	0.00004	p
59661.18658	0.00002	s	60376.58680	0.00004	s	60388.88150	0.00004	s
59661.37872	0.00002	p	60376.77960	0.00004	p	60389.07431	0.00003	p
59661.57086	0.00002	s	60376.97100	0.00004	s	60389.26571	0.00003	s
59661.76294	0.00002	p	60377.16383	0.00004	p	60389.45846	0.00003	p
59661.95514	0.00003	s	60377.35524	0.00004	s	60389.64997	0.00003	s
59662.14715	0.00002	p	60377.54803	0.00004	p	60389.84260	0.00002	p
59662.33938	0.00003	s	60377.73947	0.00004	s	60390.03422	0.00002	s
59662.53134	0.00002	p	60377.93221	0.00004	p	60390.22674	0.00002	p
59662.72357	0.00003	s	60378.12371	0.00004	s	60390.41848	0.00002	s
59662.91558	0.00002	p	60378.31640	0.00003	p	60390.61089	0.00002	p
59663.10771	0.00002	s	60378.50796	0.00003	s	60390.80268	0.00001	s
59663.29987	0.00002	p	60378.70060	0.00003	p	60390.99507	0.00002	p
59663.49192	0.00002	s	60378.89224	0.00002	s	60391.18684	0.00002	s
59663.68408	0.00002	p	60379.08478	0.00003	p	60391.37923	0.00002	p
59663.87614	0.00002	s	60379.27650	0.00002	s	60391.57106	0.00002	s
59664.06825	0.00002	p	60379.46895	0.00003	p	60391.76345	0.00002	p
59664.26030	0.00002	s	60379.66071	0.00002	s	60391.95535	0.00002	s
60367.75015	0.00002	s	60379.85316	0.00002	p	60392.14765	0.00002	p
60367.94220	0.00003	p	60380.04490	0.00002	s	60392.33968	0.00002	s
60368.13435	0.00001	s	60380.23740	0.00003	p	60392.53182	0.00002	p
60368.32640	0.00002	p	60380.42912	0.00002	s	60392.72396	0.00002	s
60368.51856	0.00002	s	60380.62159	0.00002	p	60392.91599	0.00002	p
60368.71063	0.00002	p	60380.81337	0.00002	s	60393.10822	0.00003	s
60368.90278	0.00002	s	60381.00578	0.00002	p	60393.30019	0.00003	p
60369.09486	0.00002	p	60381.19755	0.00002	s	60393.49248	0.00003	s
60369.28701	0.00002	s	60381.77428	0.00004	p	60393.68442	0.00003	p
60369.47908	0.00002	p	60381.96593	0.00003	s	60393.87674	0.00003	s
60369.67121	0.00002	s	60382.15850	0.00003	p	60394.06870	0.00002	p
60369.86330	0.00002	p	60382.35013	0.00002	s	60394.26092	0.00003	s
60370.05542	0.00002	s	60382.54277	0.00003	p	60394.45295	0.00003	p
60370.24757	0.00002	p	60382.73429	0.00002	s	60394.64512	0.00003	s
60370.43961	0.00002	s	60382.92704	0.00003	p			

The analysis reveals a cyclic variation with a semi-amplitude of 0.0256 ± 0.0007 day and a modulation period of 56.84 ± 0.08 yr. From this model, the minimum mass of the third body is estimated to be $0.63 \pm 0.02 M_{\odot}$.

An alternative explanation for cyclic $(O-C)$ variations involves magnetic activity in one or both components, as proposed by Applegate (1992). In this scenario, orbital period changes arise due to cyclic variations in the stellar quadrupole

Table 4
Minima Times for BI CVn were Obtained from the $O - C$ Gateway Database (Paschke & Brat 2006), Accessible at http://var2.astro.cz/ocgate/

Min+2400000 (HJD)	Type	Method	Reference	Min+2400000 (HJD)	Type	Method	Reference
33064.2460	s	pg	GEOS No.EB23	49869.4030	p	vis	GEOS No.EB23
33409.2600	s	pg	GEOS No.EB23	49873.4180	s	vis	BBSAG No.112
34149.2300	s	pg	GEOS No.EB23	49882.4360	p	vis	BBSAG No.112
34150.1950	p	pg	GEOS No.EB23	49889.3760	p	vis	BBSAG No.112
35599.2610	s	pg	GEOS No.EB23	50152.3673	s	CCD	IBVS No.4554
35602.3370	s	pg	GEOS No.EB23	50152.5589	p	CCD	IBVS No.4554
35604.2740	s	pg	GEOS No.EB23	50170.4400	s	vis	BBSAG No.112
35638.2660	p	pg	GEOS No.EB23	50178.3020	p	vis	BBSAG No.112
35653.2420	p	pg	GEOS No.EB23	50195.3790	s	vis	BBSAG No.112
35654.1900	s	pg	GEOS No.EB23	50211.3290	p	vis	BBSAG No.112
35659.2010	s	pg	GEOS No.EB23	50218.4450	s	vis	BBSAG No.112
36688.3120	p	pg	GEOS No.EB23	50224.3960	p	vis	BBSAG No.112
36971.7212	s	vis	Paschke & Brat (2006)	50248.4240	s	vis	BBSAG No.112
44365.2497	p	pe	IBVS No.2191	50252.4530	p	CCD	IBVS No.4554
44365.4450	s	pe	IBVS No.2191	50516.4080	p	vis	BBSAG No.115
44367.5590	p	pe	IBVS No.2191	50517.3800	s	vis	BBSAG No.115
44370.4390	s	pe	IBVS No.2191	50517.5720	p	vis	BBSAG No.115
44374.4732	p	pe	IBVS No.2590	50538.6880	p	Pe	AAVSO No.130
45769.7314	s	pe	IBVS No.2590	50546.3702	p	pe	BBSAG No.115
45770.6919	p	pe	IBVS No.2590	50547.3240	s	vis	BBSAG No.119
45770.8840	s	pe	IBVS No.2590	50581.3400	p	vis	BBSAG No.119
45773.7655	p	pe	IBVS No.2590	50599.4010	p	vis	BBSAG No.119
45773.9575	s	pe	IBVS No.2590	51250.4335	s	CCD	IBVS No.4912
45841.7611	p	pe	IBVS No.2590	51258.6944	p	CCD	IBVS No.5027
46148.3670	p	vis	BBSAG No.77	51274.6380	s	CCD	ROTSE
46173.3270	p	vis	BBSAG No.77	51277.7129	s	CCD	IBVS No.5027
46180.4496	s	pe	Demircan (1987)	51278.4700	s	CCD	BBSAG No.121
46200.4180	s	vis	BBSAG No.77	51305.3760	s	vis	BBSAG No.120
46220.4060	s	vis	BBSAG No.77	51315.3690	s	vis	BBSAG No.121
48329.5100	p	vis	BBSAG No.98	51656.3430	p	vis	BBSAG No.122
48387.5280	p	vis	BBSAG No.98	51678.4430	s	CCD	IBVS No.5296
48400.4050	s	vis	BBSAG No.98	52285.6859	p	CCD	BBSAG No.127
48500.0973	p	CCD	Hipparcos	52296.6362	s	CCD	BBSAG No.127
48681.4388	p	CCD	BAV No.60	52321.6070	s	vis	IBVS No.5543
48717.3610	s	vis	BBSAG No.102	52338.4960	s	vis	IBVS No.5543
48733.4920	s	vis	BBSAG No.102	52370.6040	p	vis	IBVS No.5543
48747.5240	p	vis	BBSAG No.102	52373.4775	s	CCD	IBVS No.5484
48791.5030	s	vis	BBSAG No.102	52408.7297	p	CCD	AAVSO No.130
49137.4860	p	CCD	IBVS No.4554	52687.1813	p	CCD	VSOLJ No.42
49479.4300	p	CCD	IBVS No.4554	52693.5265	s	CCD	IBVS No.5643
49484.4310	p	vis	GEOS No.EB23	52694.4851	p	CCD	IBVS No.5438
49502.4730	p	vis	GEOS No.EB23	52762.4909	p	pe	IBVS No.5471
49503.4390	s	vis	GEOS No.EB23	52763.4517	s	CCD	IBVS No.5668
49516.5080	s	CCD	IBVS No.4554	52764.4114	p	CCD	IBVS No.5668
49722.6325	p	pe	IBVS No.4554	52765.3727	s	CCD	IBVS No.5668
49761.4375	p	CCD	IBVS No.4554	53047.5749	p	CCD	IBVS No.5592
49761.6308	s	CCD	IBVS No.4554	53080.6175	p	CCD	IBVS No.5643
49786.4130	p	vis	GEOS No.EB23	53094.4474	p	CCD	IBVS No.5543
49797.3540	s	vis	GEOS No.EB23	53095.7933	s	CCD	IBVS No.5602
49798.5190	s	vis	GEOS No.EB23	53422.9478	p	CCD	IBVS No.5690
49799.4710	p	vis	GEOS No.EB23	53451.3784	p	pe	IBVS No.5649
49801.4000	p	vis	GEOS No.EB23	53462.5215	p	pe	IBVS No.5657
49810.4200	s	vis	GEOS No.EB23	53465.4037	s	pe	IBVS No.5657
49810.4258	s	pe	IBVS No.4554	53490.3770	s	CCD	IBVS No.5668
49827.3260	s	vis	GEOS No.EB23	53729.5475	p	pe	IBVS No.5754
49830.5920	p	vis	GEOS No.EB23	53883.6162	p	CCD	IBVS No.5814
49841.3410	p	vis	GEOS No.EB23	54137.9636	p	CCD	IBVS No.5806

Table 4
(Continued)

Min+2400000 (HJD)	Type	Method	Reference	Min+2400000 (HJD)	Type	Method	Reference
49843.4500	s	vis	GEOS No.EB23	54177.7284	s	CCD	IBVS No.5820
49858.4600	s	vis	GEOS No.EB23	54184.4517	p	CCD	IBVS No.5795
49863.4330	s	vis	GEOS No.EB23	54211.3464	p	CCD	IBVS No.5795
54871.8029	p	CCD	IBVS No.5938	57413.5532	s	CCD	BRNO
54888.9012	s	CCD	IBVS No.5894	57465.4213	s	CCD	IBVS No.6196
54922.3271	s	CCD	IBVS No.5898	57465.6096	p	CCD	IBVS No.6197
54937.5033	p	CCD	IBVS No.5898	57489.4319	p	CCD	IBVS No.6198
54957.6763	s	CCD	IBVS No.5894	57489.6259	s	CCD	IBVS No.6199
54971.5196	s	CCD	IBVS No.5918	57824.0795	p	CCD	VSOLJ No.64
55249.4816	p	CCD	IBVS No.5980	57824.2725	s	CCD	VSOLJ No.64
55251.7874	p	CCD	IBVS No.5974	57825.4265	s	CCD	IBVS No.6244
55283.6760	p	CCD	IBVS No.5945	57825.6156	p	CCD	IBVS No.6244
55309.4183	p	CCD	IBVS No.5959	57829.4586	p	CCD	IBVS No.6244
55311.3397	p	CCD	IBVS No.5980	57829.6504	s	CCD	IBVS No.6244
55315.3737	s	CCD	BRNO	57846.3632	p	CCD	BRNO
55336.3077	p	CCD	AAVSO No.130	57899.7702	p	CCD	IBVS No.6234
55593.9265	s	CCD	IBVS No.6018	58124.1474	p	CCD	VSOLJ No.66
55606.4136	p	CCD	IBVS No.5980	58202.3359	s	CCD	BAV No.31
55622.9344	p	CCD	IBVS No.5992	58202.5286	p	CCD	BAV No.31
55643.2990	p	CCD	IBVS No.6044	58304.7281	p	CCD	AAVSO No.462
55669.4261	p	CCD	IBVS No.6010	58540.4398	s	CCD	BAV No.33
55669.6163	s	CCD	IBVS No.6010	58540.6344	p	CCD	BAV No.33
55672.4987	p	CCD	IBVS No.6044	58545.4370	s	CCD	BAV No.30
55685.7485	s	CCD	IBVS No.5992	58545.6280	p	CCD	BAV No.52
55700.3526	s	CCD	IBVS No.6010	58924.4608	p	CCD	BAV No.52
55700.5462	p	CCD	IBVS No.6010	58924.6532	s	CCD	BAV No.52
55989.8547	p	CCD	IBVS No.6029	58927.3412	s	CCD	BAV No.52
56012.5240	p	CCD	IBVS No.6048	58927.5346	p	CCD	BAV No.52
56051.7145	p	CCD	IBVS No.6029	58939.4444	p	CCD	BAV No.52
56381.7513	p	CCD	Nelson et al. (2014)	58977.4827	p	CCD	BRNO
56385.7841	s	CCD	Nelson et al. (2014)	59157.6792	p	CCD	BRNO
56395.3902	s	CCD	Nelson et al. (2014)	59280.4340	s	CCD	BAV No.60
56395.5824	p	CCD	Nelson et al. (2014)	59280.6239	p	CCD	BAV No.60
56400.5747	p	CCD	IBVS No.6084	59281.3927	p	CCD	BRNO
56407.4389	p	CCD	IBVS No.6084	59286.3875	p	CCD	BRNO
56423.4374	s	CCD	IBVS No.6167	59298.2984	p	CCD	BAV No.60
56729.4634	p	CCD	IBVS No.6149	59298.4917	s	CCD	BAV No.60
56729.6559	s	CCD	IBVS No.6149	59304.4445	p	CCD	BAV No.60
56734.4597	p	CCD	IBVS No.6149	59304.6387	s	CCD	BAV No.60
57036.6389	s	CCD	IBVS No.6167	59305.4064	s	CCD	BAV No.60
57056.6188	s	CCD	IBVS No.6152	59305.5980	p	CCD	BAV No.60
57064.6860	s	CCD	OEJV No. 172	59329.4200	p	CCD	BAV No.55
57070.4505	s	CCD	IBVS No.6167	59339.2154	s	CCD	VSOLJ No.91
57125.3925	s	CCD	IBVS No.6191, This study	59402.4187	p	CCD	BRNO
57125.5822	p	CCD	IBVS No.6191, This study	59527.6768	p	CCD	BAV No.69
57136.5349	s	CCD	IBVS No.6209	59604.5132	p	CCD	BAV No.69
57137.4950	p	CCD	IBVS No.6209	59640.6223	p	CCD	BRNO
57141.3373	p	CCD	IBVS No.6191, This study	59651.7722	p	CCD	OEJV 234
57141.5297	s	CCD	IBVS No.6191, This study	59665.5961	p	CCD	BRNO
57151.3264	p	CCD	IBVS No.6191, This study	59772.4147	p	CCD	VSOLJ No.108
57151.5190	s	CCD	IBVS No.6191, This study	…	…	…	…
57152.4788	p	CCD	IBVS No.6191, This study	…	…	…	…

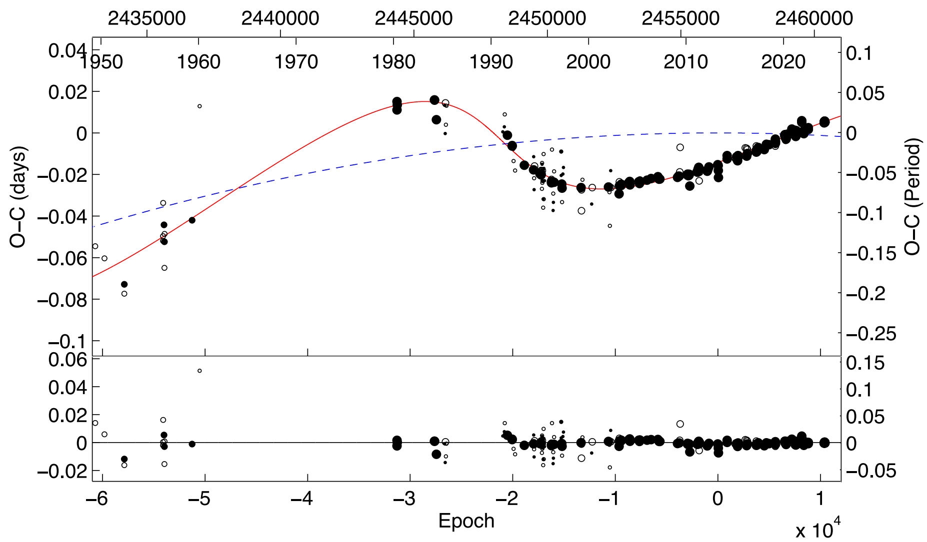

Figure 4. The best-fitting downward parabolic (blue dashed line) and sinusoidal curves (red solid line) superimposed on $(O-C)$ diagram of BI CVn.

moment ΔQ, expressed as (Lanza & Rodonò 2002)

$$\frac{\Delta P}{P} = -9\frac{\Delta Q}{Ma^2}, \tag{4}$$

where M is the mass of the magnetically active star, and a is the orbital separation. The computed values of ΔQ for the two components are 5.2×10^{49} g cm^2 and 1.3×10^{50} g cm^2, respectively. These values are significantly lower than the typical range of 10^{51}–10^{52} g cm^2 expected for the Applegate mechanism to be viable (Lanza & Rodonò 1999), indicating that magnetic activity is unlikely to account for the observed cyclic behavior in BI CVn.

5. Absolute Dimensions

The absolute parameters of eclipsing binary star systems can be determined through the simultaneous analysis of their radial velocity and light curves. For BI CVn, the photometric mass ratio of the components ($q = M_2/M_1$) was determined to be 2.436 ± 0.003. The distance between the centers of mass of the component stars was derived as $a = 2.80 \pm 0.01 R_\odot$, as presented in Table 2. Using Kepler's third law, expressed as ($M_1 + M_2 = a^3/P^2$), the masses of the components were calculated to be $M_1 = 0.58 \pm 0.01\ M_\odot$ and $M_2 = 1.42 \pm 0.02 M_\odot$.

Applying the definition of fractional radii, $r_{1,2} = R_{1,2}/a$, together with the mean fractional radii from Table 2 ($r_1 = 0.3066 \pm 0.0005$ and $r_2 = 0.4698 \pm 0.0005$), the radii of the primary and secondary components were calculated as $R_1 = 0.88 \pm 0.01 R_\odot$ and $R_2 = 1.31 \pm 0.01 R_\odot$, respectively. These absolute parameters are summarized in Table 6. The bolometric corrections (BC) are taken from Flower (1996) based on the effective temperatures of the component stars. The bolometric absolute magnitude of the Sun is assumed to be $M_{\odot,\mathrm{bol}} = 4.75$.

Table 5
$(O-C)$ Analysis Results for BI CVn

Parameter	Unit	Value
T_0	(BJD)	2456385.9929 ± 0.0018
P_s	(day)	0.38420923 ± 0.00000012
Q (x10^{-10})	(day)	−0.1217 ± 0.0001
A	(day)	0.0256 ± 0.0007
T_3	(BJD)	2448175 ± 301
P_3	(yr)	56.84 ± 0.08
e_3		0.43 ± 0.09
ω_3	(deg)	173 ± 6
$a_{12} \sin i_3$	(au)	4.89 ± 0.13
$f(M_3)$	($M_\odot$)	0.036 ± 0.002
$M_{3\,\mathrm{min}}$	($M_\odot$)	0.63 ± 0.02

The interstellar reddening was estimated using the infrared dust emission maps from Schlafly & Finkbeiner (2011), yielding a color excess of $E_{(B-V)} = 0.0113 \pm 0.0003$. Using this color excess and the apparent magnitude ($V = 10.31$) at maximum light, the distance to the system was calculated to be 219 ± 10 pc. This value aligns well with the distance of 221 pc derived from the trigonometric parallax (4.52 mas) reported in Gaia Data Release 3 (DR3; Gaia Collaboration et al. 2021).

6. Evolution Models and Discussion

The evolution models of BI CVn were developed using the Binary Star Evolution (BSE) code created by Hurley et al. (2002). This fast and efficient code is designed for simulating the evolution of binary star systems. It provides detailed modeling of tidal interactions, including the circularization of eccentric orbits and synchronization of orbit and spin motion.

Table 6
Astrophysical Parameters for BI CVn

Parameter	Primary	Secondary
M ($M_\odot$)	0.58 ± 0.01	1.42 ± 0.02
R ($R_\odot$)	0.88 ± 0.01	1.31 ± 0.01
log g (cgs)	4.28 ± 0.01	4.34 ± 0.02
T (K)	6125 ± 100	6093 ± 100
L ($L_\odot$)	0.98 ± 0.08	2.13 ± 0.02
M_bol	4.78 ± 0.05	3.93 ± 0.08
a ($R_\odot$)	2.80 ± 0.01	…
BC	−0.029	−0.036
M_v	4.805 ± 0.044	3.971 ± 0.081
$E(B-V)$ ($^{\rm m}$)	0.0113 ± 0.0003	…
d (pc)	219 ± 10	…
$d_{\rm Gaia}$ (pc)	221	…

The code also accounts for angular momentum loss mechanisms, such as gravitational radiation and magnetic braking. In the modeling process, it is assumed that the contact binaries consist of detached components. The models were constructed using the absolute parameters given in Table 6.

Estimating the initial parameters of the components in BSE models is challenging. However, it can be assumed that the initial masses of the components were larger than their current masses. After some experimentation, we chose the initial masses of the components as $1.64M_\odot$ and $0.69M_\odot$, the initial period as $P_0 = 1.87$ day, and the mass fraction of heavy elements as $Z = 0.02$. The mass transfer pattern proposed by Stępień & Kiraga (2015) is considered during the semi-detached and contact phases. The simplified dynamo model of Eggleton (2006) was used to account for mass loss due to magnetic braking and stellar winds. Parameters related to dynamo-origin mass and angular momentum loss were taken as cml, chl 0.2 and 1.0, respectively. Calculations began at the zero-age main sequence (ZAMS), with the eccentricity assumed to be zero. To evaluate the compatibility of the modeling with the system, the mass, radius, period, relative radii, and positions of the model and the system on the Hertzsprung-Russell (HR) diagram were analyzed. During the contact phase, special attention was given to the agreement between the system and the model.

In panel (a) of Figure 5, the positions of the components on the log R–M plane are plotted along with their evolution tracks. The filled and open symbols represent the primary and secondary stars, respectively. The black solid line represents the evolutionary track of the primary component, while the black dashed line shows the change in the Roche lobe radius of the primary component. Similarly, the solid turquoise line represents the evolutionary track of the secondary component, and the dashed turquoise line shows the Roche lobe radius of the secondary component. The ZAMS is displayed as a blue dashed line, and the terminal-age main sequence is represented as a purple dashed line. The evolutionary tracks of the components start from the points marked with plus signs. The point labeled (SD) indicates where the initially massive component fills its Roche lobe, initiating the semi-detached phase. After this point, the massive component transfers mass to the smaller component, causing the smaller component to move up along the ZAMS. During mass exchange, the component gaining mass becomes younger, while the one losing mass ages. At point (C), both components simultaneously fill their Roche lobes and enter the contact phase. The mass-time diagram in panel (b) shows the changes in the theoretical masses of the components and the total mass. The turquoise solid line represents the initially massive component, and the black solid line represents the initially smaller component. The red solid line shows the change in total mass. The dashed horizontal lines labeled (1) and (2) indicate the observed masses of the components. The vertical blue line labeled (SD) marks when the initially massive component fills its Roche lobe, while the vertical black dashed line labeled (C) indicates when both components fill their Roche lobes and the system enters the contact phase. The dashed red line labeled (A) represents the predicted age of the system in the model. After the contact phase, the dashed horizontal lines (1) and (2) intersect the theoretical masses simultaneously at the red vertical line (A). In panel (c), the changes in the theoretical radii of the components over time are shown. The solid turquoise line indicates the radius of the initially massive component, and the dashed turquoise line represents its Roche lobe radius. The black solid line shows the radius of the initially smaller component, and the dashed black line indicates its Roche lobe radius. The vertical blue line marks when the initially massive component fills its Roche lobe, while the vertical black dashed line marks when both components fill their Roche lobes. The dashed red line labeled (A) represents the predicted age of the system in the model. Panel (d) shows the change of the theoretical orbital period of the system versus time. The black dashed horizontal line represents the observed orbital period. The vertical blue dashed line marks when the initially massive component fills its Roche lobe, and the vertical black dashed line marks when both components fill their Roche lobes and the system enters the contact phase. The dashed red line represents the predicted age of the system in the model. After the contact phase, the theoretical and observational curves intersect at approximately 2.65 Gyr. Panel (e) shows the system's status on the HR diagram. The black dot indicates the initially massive component, and the open dot represents the initially smaller component. The black and turquoise solid lines show the evolutionary paths produced by the model for the initially massive and smaller components, respectively. When the system reaches the contact phase, energy transfer between the components causes the temperatures to equalize and the luminosities to converge, resulting in sharp turns in the diagram.

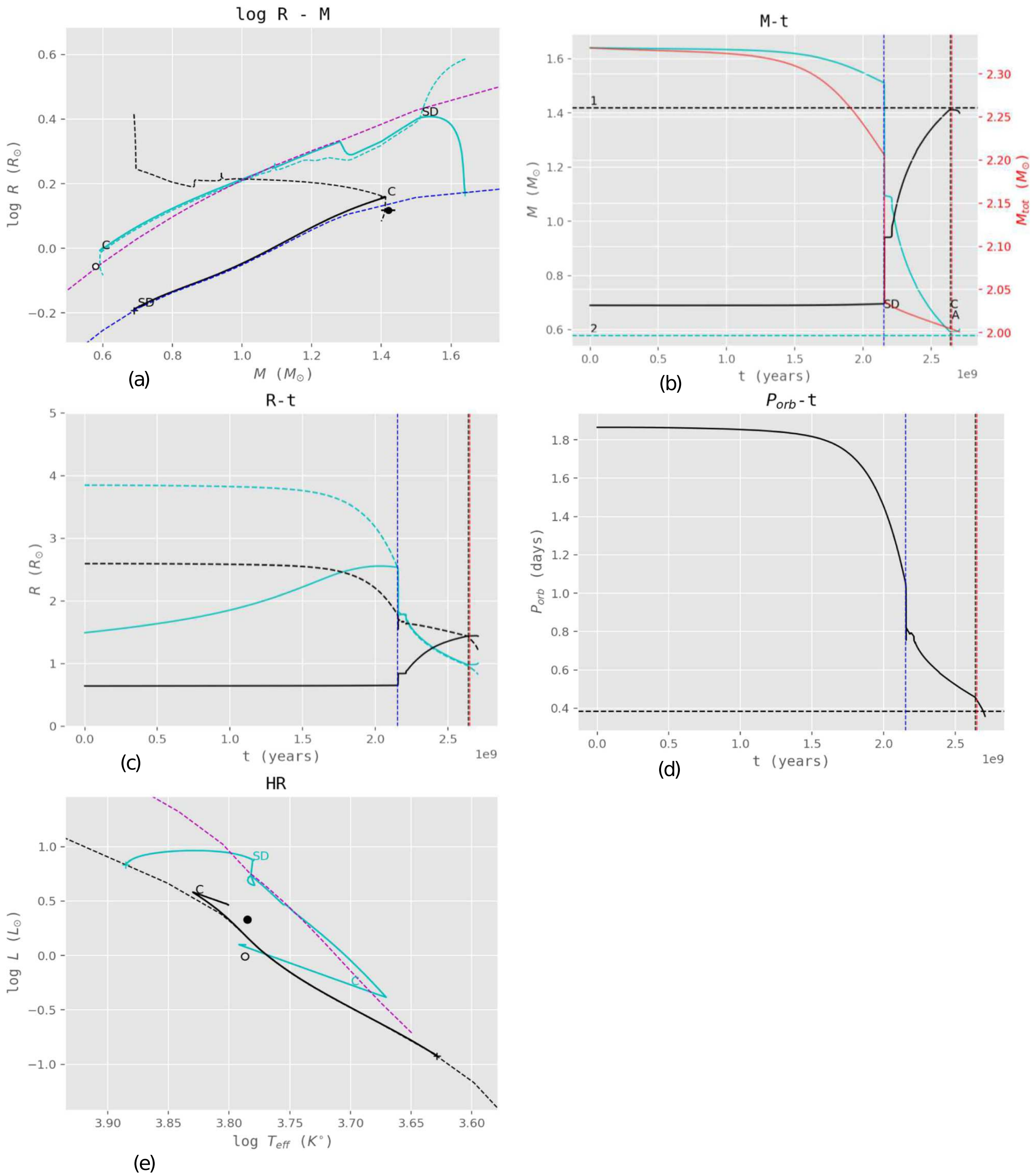

Figure 5. Evolutionary tracks for the best model of BI CVn. The data for BI CVn are represented as squares. Panel (a) shows the evolution in the log *R*–*M* plane. Panel (b) shows the change of the theoretical masses of the components and the total mass. Panel (c) shows the change of theoretical radii of the components over time. Panel (d) shows the change in the theoretical orbital period of the system. Panel (e) shows the status of the system in the HR diagram.

7. Results

In this study, the radial velocity and *BVR* light curves of BI CVn were analyzed together using the WD method, and the orbital parameters of the system and the fundamental astrophysical parameters of the components were calculated (Tables 2 and 6). The masses of the components in BI CVn were calculated as $0.58 \pm 0.01 M_{\odot}$ and $1.42 \pm 0.02 M_{\odot}$ for the primary and secondary components, respectively, and their radii were calculated as $0.88 \pm 0.01 R_{\odot}$ and $1.31 \pm 0.01 R_{\odot}$, respectively. According to these results, the hotter component of the system is less massive and has the smaller radius. This shows that the more massive and cooler component of the system evolves more than the less massive and hotter component. Additionally, the temperature difference between the components is very small ($\Delta T = 32$ K), indicating that the system is in thermal contact. The degree of contact of the system was determined to be $f = 17.1\%$. The calculated distance of 219 pc is in good agreement with the Gaia DR3 value.

Additionally, the change in the orbital period of the system was investigated by $(O - C)$ analysis. This was accomplished by combining new minimum times with all previously published minimum times from the literature. According to the $(O - C)$ analysis results, the quadratic term representing the parabolic change was calculated as $Q = -0.1217\ (\pm 0.0001) \times 10^{-10}$ day. This result corresponds to a decrease in the orbital period of $dP/dt = -2.3239\ (\pm\ 0.0001) \times 10^{-8}$ day yr^{-1}, indicating that the orbital period of BI CVn decreases by 0.2 s per century. The mass transfer rate from the more massive component to the less massive component was determined as $1.97 \times 10^{-8} M_{\odot}$ yr^{-1}. The shortening in the orbital period may be a sign of an impending merger in a contact binary. To describe the asymmetric sinusoidal shaped periodic variation in the $O - C$ diagram, LITE was applied assuming the existence of a tertiary component around BI CVn. Accordingly, it was found that the orbital semimajor axis length of the possible third component was approximately 4.89 ± 0.13 au, and its period was approximately 56.84 ± 0.08 yr. The orbital period of the third component is longer than the value of about 27 yr reported by Qian et al. (2008). The minimum mass of the possible third unseen component in the system was calculated as $0.63 \pm 0.02 M_{\odot}$. It is most likely a cool dwarf star.

Possible evolution scenarios of the system were modeled with BSE code. The variation in parameters such as mass, radius, and period throughout the system's evolution was determined in a manner consistent with their current values. According to the modeling results, the initially more massive component filled the Roche lobe at about 2.1 Gyr and the system reached the semi-detached phase. The system evolved to approximately the observed masses and radii at 2.65 Gyr. The probable merger age was estimated to be about 2.70 Gyr.

Acknowledgments

The authors thank the anonymous referee who helped to improve the early version of the manuscript with his/her very useful comments. We gratefully acknowledge the observing time granted at the Ulupınar Observatory of Çanakkale Onsekiz Mart University. This study utilized observational data obtained through a project supported by the Scientific and Technological Research Council of Türkiye (TÜBİTAK) under grant No. 114F166. This paper includes data collected by the Transiting Exoplanet Survey Satellite (TESS) mission. Funding for TESS is provided by the NASA Science Mission Directorate. TESS data presented in this work were obtained from the Mikulski Archive for Space Telescopes (MAST). This work also presents results from the Gaia mission, a project of the European Space Agency (ESA). Gaia data are processed by the Gaia Data Processing and Analysis Consortium (DPAC). Funding for DPAC is provided by national institutions, in particular those participating in the Gaia MultiLateral Agreement (MLA). The Gaia mission website is: https://www.cosmos.esa.int/gaia, and the Gaia archive is accessible at: https://archives.esac.esa.int/gaia. Additionally, this research made use of the SIMBAD database, operated at CDS, Strasbourg, France, and NASA's Astrophysics Data System Bibliographic Services.

References

Applegate, J. H. 1992, ApJ, 385, 621
Bulut, İ., & Aşkın, G. 2022, NewA, 90, 101668
Bulut, İ., Kabaş, A., Nehir, Ç., et al. 2017, IBVS, 6191, 1
Demircan, O. 1987, Ap&SS, 135, 169
Eggleton, P. 2006, Evolutionary Processes in Binary and Multiple Stars, 40 (Cambridge: Cambridge Univ. Press)
Filatov, G. S. 1960, ATsir, 215, 20
Flower, P. J. 1996, ApJ, 469, 355
Gaia Collaboration, Brown, A. G. A., Vallenari, A., et al. 2021, A&A, 649, A1
Hurley, J. R., Tout, C. A., & Pols, O. R. 2002, MNRAS, 329, 897
Irwin, J. B. 1959, AJ, 64, 149
Kwee, K. K., & van Woerden, H. 1956, BAN, 12, 327
Lanza, A. F., & Rodonò, M. 1999, A&A, 349, 887
Lanza, A. F., & Rodonò, M. 2002, AN, 323, 424
Liu, X., & Tan, H. 1984, IBVS, 2590, 1
Liu, X. F., & Tan, H. S. 1988, AcASn, 29, 16
Lu, W. X. 1988, AcApS, 8, 259
Lucy, L. B. 1968, ApJ, 151, 1123
Maceroni, C., & van't Veer, F. 1996, A&A, 311, 523
Motl, D., 2007 C-Munipack Project v1.2.32
Nelson, R. H., Şenavci, H. V., Baştürk, Ö., & Bahar, E. 2014, NewA, 29, 57
O'Connell, D. J. K. 1951, PRCO, 2, 85
Paschke, A., & Brat, L. 2006, OEJV, 23, 13
Prša, A., & Zwitter, T. 2005, ApJ, 628, 426
Qian, S. B., He, J. J., Liu, L., Zhu, L. Y., & Liao, W. P. 2008, AJ, 136, 2493
Samec, R. G., Labadorf, C. M., Hawkins, N. C., Faulkner, D. R., & Van Hamme, W. 2011, AJ, 142, 117
Schlafly, E. F., & Finkbeiner, D. P. 2011, ApJ, 737, 103
Stępień, K., & Kiraga, M. 2015, A&A, 577, A117
Tylenda, R., Hajduk, M., Kamiński, T., et al. 2011, A&A, 528, A114
van Hamme, W. 1993, AJ, 106, 2096
vant Veer, F. 1979, A&A, 80, 287
Wilson, R. E., & Devinney, E. J. 1971, ApJ, 166, 605
Zasche, P., Liakos, A., Niarchos, P., et al. 2009, NewA, 14, 121
Zhukov, G. V. 1982, IBVS, 2191, 1